Kinetics and Mechanistic Studies of the Atmospheric Oxidation of Alkynes

Laurence Y. Yeung, Michael J. Pennino, Angela M. Miller, and Matthew J. Elrod*

Department of Chemistry, Oberlin College, Oberlin, Ohio 44074

Received: October 5, 2004; In Final Form: November 23, 2004

Kinetics studies of the OH-initiated oxidation of 2-butyne, propyne, and acetylene were conducted at 100 Torr and 298 K using turbulent flow chemical ionization mass spectrometry. The major oxidation products were identified, and with the aid of supporting electronic structure thermodynamics calculations, a general OH-initiated oxidation mechanism for the alkynes is proposed. The major product branching ratio and the product-forming rate constants for the 2-butyne-OH adduct + O_2 reaction were experimentally determined as well. The atmospheric implications of the chemical oxidation mechanism and kinetics results are discussed.

Introduction

Unsaturated hydrocarbons play an important role in the production of ground level ozone, a key constituent of photochemical smog. Atmospheric alkenes derive from large biogenic and anthropogenic emission sources.[1] Alkynes, on the other hand, are believed to be emitted almost entirely from two major anthropogenic sources: biomass burning processes[2−5] and automobile tailpipe emissions.[6−9] Previous studies of automobile exhaust have found acetylene emissions to be comparable to that of ethylene.[7−9] A biogenic marine source of atmospheric acetylene has been proposed by Kanakidou and co-workers,[10] though its contribution to global acetylene levels is probably negligible compared to that due to anthropogenic sources.[3,11] Recent atmospheric measurements have determined acetylene concentrations of 6 and 17 ppbv above Boston and Los Angeles, respectively, which are comparable to that of ethylene. [12] In remote areas, however, atmospheric acetylene concentrations have typically been found to be under 0.6 ppbv.[11] Propyne, 1-butyne, and 2-butyne have also been detected in the atmosphere.[6,9]

The atmospheric oxidation of both saturated and unsaturated hydrocarbons is usually initiated by reaction with OH. The initial step in the OH-initiated oxidation of alkanes in the troposphere occurs primarily through hydrogen atom abstraction. The general mechanism is shown in reactions 1−3, where R is any alkyl group

$$R-H + OH \rightarrow R + H_2O \quad (1)$$

$$R + O_2 \rightarrow R-O_2 \quad (2)$$

$$R-O_2 + NO \rightarrow R-O + NO_2 \quad (3a)$$

$$\rightarrow R-ONO_2 \quad (3b)$$

It is the conversion of NO to NO_2 in the hydrocarbon oxidation mechanism (reaction 3a for the alkanes) that directly leads to tropospheric ozone production

$$NO_2 + h\nu \rightarrow NO + O \quad (4)$$

$$O + O_2 \rightarrow O_3 \quad (5)$$

Although the rate of reaction 1 generally increases with increasing alkane chain length,[12] recent work by Eberhard and Howard has shown that the rate of reaction 3 is independent of the length and degree of branching of the alkyl chain.[13]

Alkenes, on the other hand, undergo oxidation by OH primarily through addition. However, the abstraction pathway can become significant at the elevated temperatures characteristic of combustion environments. The addition pathway is outlined in reactions 6−8 where R and R′ are any alkyl group

$$R-CH{=}CH-R' + OH \rightarrow R-CH(OH)-CH-R' \quad (6)$$

$$R-CH(OH)-CH-R' + O_2 \rightarrow R-CH(OH)-CH(O_2)-R' \quad (7)$$

$$R-CH(OH)-CH(O_2)-R' + NO \rightarrow R-CH(OH)-CH(O)-R' + NO_2 \quad (8a)$$

$$\rightarrow R-CH(OH)-CH(ONO_2)-R' \quad (8b)$$

The rate of reaction 6 is found to increase with increasing alkene chain length.[12] As with the alkanes, reaction 8 was recently found to be independent of the size and degree of branching of the alkyl chains attached to the double bond.[14]

The traditional view of the OH-initiated oxidation mechanism of alkynes is that it should be similar to that of the alkenes, with alkynes contributing to tropospheric ozone production via a process similar to reactions 6−8.[1] However, definitive kinetics results exist only for the initial OH reaction step. As expected, the OH addition pathway appears to dominate without any evidence of a hydrogen atom abstraction channel.[15] In 1985, using a laser-induced fluorescence technique to monitor OH in the presence of acetylene and O_2, Schmidt et al. identified rapid OH regeneration, presumably due to reaction of the C_2H_2−OH adduct with O_2.[16] They also tentatively identified a vinoxy radical intermediate (HC(=O)−CH_2) resulting from the C_2H_2 + OH reaction, as well as the formation of the stable product glyoxal (ethanedial; O=HC−CH=O) in the presence of O_2.

* To whom correspondence should be addressed. E-mail: matthew.elrod@oberlin.edu Telephone: (440) 775-6583. Fax: (801) 697-4917.

10.1021/jp0454671 CCC: $30.25
Published on Web 02/12/2005

In 1986, Hatakeyama et al. presented the first comprehensive product analyses of the oxidation of acetylene, propyne, and 2-butyne using an environmental chamber and FT-IR detection.[17] Glyoxal and formic acid production resulting from the OH-initiated oxidation of acetylene were observed in any O_2-only atmosphere (no NO_x). Hatakeyama et al. consequently proposed two primary mechanisms through which the acetylene-OH adduct could react with O_2.

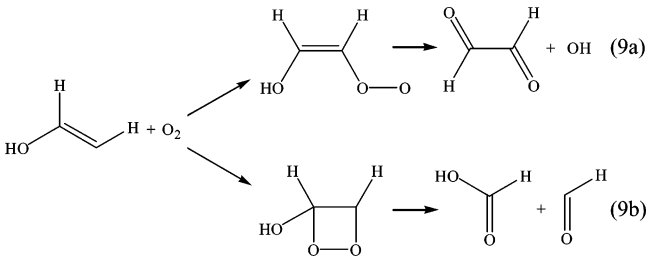

In reaction 9a, molecular oxygen can add to the acetylene−OH adduct to form a peroxy radical, which eventually leads to the production of glyoxal and the regeneration of OH (which is necessary to explain the results of Schmidt et al.[16]). They further proposed that molecular oxygen can also add to the double bond to form a four-membered cyclic intermediate in reaction 9b, which then decomposes to formic acid and formyl radical. Hatakeyama et al. also observed stable products consistent with their proposed mechanism for the propyne system, methylglyoxal (2-oxo-propional) and formic acid, and the 2-butyne system, biacetyl (butane-2,3-dione) and acetic acid. However, for the propyne system, no acetic acid was observed, which was interpreted as evidence that OH addition occurs preferentially at the terminal carbon atom.

It is important to note that the major product channel of the $C_2H_2-OH + O_2$ reaction proposed by Hatakeyama et al. involves the formation of a peroxy radical intermediate (reaction 9a).[17] It is the reaction of peroxy radicals with NO that drives the OH-initiated oxidation of alkanes and alkenes to contribute to tropospheric ozone production. To ascertain whether the expected peroxy radical intermediate was present in their reaction system, Hatakeyama et al. also performed experiments in the presence of NO_x. Interestingly, no significant change in the oxidation products was observed. This result was interpreted as a possible indication that alkynes may undergo a substantially different oxidation mechanism than the alkanes and alkenes. In particular, if the oxidation mechanism does not require reaction with NO to reach stable oxidation products, the alkynes may not substantially contribute to tropospheric ozone production. However, since the environmental chamber experiments of Hatakeyama et al. were carried out on the several minute time scale, an atmospherically significant lifetime for the peroxy radical intermediate could not be ruled out.

Siese and Zetzsch also investigated the OH-initiated oxidation of acetylene using OH cycling methods.[18] They also found rapid OH regeneration in the presence of oxygen (no NO_x). Using the mechanism and the relative rates of reactions 9a and 9b reported by Hatakeyama et al.,[17] Siese and Zetzsch estimated the rate constant for the reaction of the C_2H_2-OH adduct with O_2 to be about 4×10^{-12} cm^3 molecule^{-1} s^{-1} at room temperature, independent of pressure, with most of the reaction leading to the regeneration of OH. Using the assumption that the formation kinetics of the stable oxidation products observed by Hatakeyama et al. correlate with the observed OH regeneration kinetics observed by Siese and Zetzsch, the previous results are consistent with a short lifetime for any peroxy radical intermediate.

More recently, Bohn and Zetzsch, using OH cycling measurements and modeling calculations, postulated the existence of HO_2 formation in the oxidation of acetylene in the absence of NO.[19] They attributed the HO_2 formation to the reaction of the formyl radical (produced in reaction 9b) with O_2. This result suggests that reaction 9b may indirectly contribute to tropospheric ozone production, as HO_2 rapidly reacts with NO to produce NO_2.

It is apparent that the previous work on the OH-initiated oxidation of the alkynes indicates the possibility of a fundamentally different oxidation mechanism than that which has been observed for the alkanes and alkenes. In particular, the previous studies were not able to identify the presence or influence of peroxy radicals in the mechanism. This aspect of the mechanism is most important, as it is the reaction of peroxy radicals with NO that directly leads to the ozone-producing nature of the alkane and alkene oxidation mechanisms.

This article describes an experimental and computational investigation aimed at the elucidation of the OH-initiated oxidation of alkynes (including the attempted direct identification of peroxy radicals potentially produced in this process). Kinetics and product measurements were conducted at 100 Torr and 298 K using the turbulent flow-chemical ionization mass spectrometric (TF−CIMS) approach for acetylene, propyne, and 2-butyne. In conjunction with experimental results, electronic structure calculations were carried out on the relevant species in order to propose a general atmospheric alkyne oxidation mechanism and thus assess the role of alkynes in the production of tropospheric ozone.

Experimental Methods

Turbulent Flow Reactor. A schematic of the experimental apparatus is presented in Figure 1 and is similar to that used in our previous kinetics study of the NO reaction with hydroxyalkylperoxy radicals derived from the OH-initiated oxidation of alkenes.[14] The flow tube was constructed with 2.2 cm i.d. Pyrex tubing and was 100 cm in total length. A large flow of ultrahigh-purity nitrogen carrier gas (99.999%, oxygen < 5 ppm; approximately 30 STP L min^{-1}) was injected at the rear of the flow tube. The gases necessary to generate OH were introduced though a 10 cm long, 12.5 mm diameter sidearm located at the rear of the tube. The alkyne-OH adducts were prepared using the following reactions: To generate fluorine atoms, a dilute

$$CF_4 \rightarrow xF + CF_{4-x} \quad (10)$$

$$F + H_2O \rightarrow HF + OH \quad (11)$$

$$OH + R-C\equiv C-R' \rightarrow R-C(OH)=C-R' \quad (12)$$

mixture of CF_4/He was passed through a microwave discharge produced by a 5-mm diameter Beenakker cavity operating at 50 W. The dilute mixture was obtained by combining a 5.0 STP L min^{-1} flow of helium (99.999%), which had passed through a silica gel trap immersed in liquid nitrogen, with a 1.0 STP mL min^{-1} flow of a 2% CF_4 (99.9%)/He mixture. Excess water ([H_2O] $\sim 2 \times 10^{14}$ molecule cm^{-3}) was added downstream of the fluorine atom source by flowing ~10 STP mL min^{-1} He through a water reservoir held at ~298 K. This ensured that no fluorine atoms were introduced into the main flow. For product identification experiments, the alkyne and O_2 were added to the sidearm, downstream of the OH source. For kinetics experiments, the alkyne was added to the main flow tube, upstream of the OH source, and O_2 was added via an encased movable injector. The encasement (made from cor-

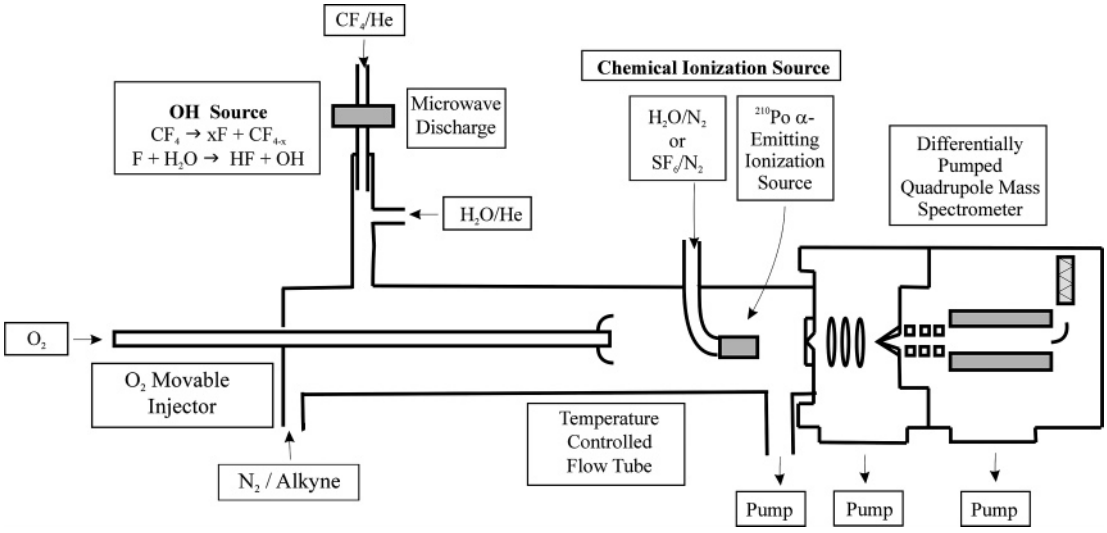

Figure 1. TF−CIMS apparatus setup for kinetics experiments.

rugated Teflon tubing) was used so that the injector could be moved to various injector positions without breaking any vacuum seals. A fan-shaped Teflon device was placed at the end of the injector in order to enhance turbulent mixing. The ^{210}Po α-emitting ionization source was placed between the flow tube and the inlet to the CIMS. Most of the flow tube gases were removed at the CIMS inlet by a 31 L s^{-1} roughing pump. All gas flows were monitored with calibrated mass flow meters. The flow tube pressure was measured upstream of the ionization source using a 0−1000 Torr capacitance manometer. The temperature was determined at both the entrance and exit points of the temperature regulated region of the flow tube using Cu-constantan thermocouples. For all experiments, the pressure was held at 100 ± 1 Torr and temperature was held at 298 ± 2 K, which reflected variations in the room temperature.

To guide kinetic modeling, it is necessary to have an estimate for the approximate concentration of OH produced by radical source. Absolute OH concentrations (in the absence of the alkyne) were determined by titrating OH with NO_2 to produce HNO_3. The absolute HNO_3 concentrations were determined by the calibration of the HNO_3 mass spectrometer signal using a bubbler containing 60% HNO_3 solution by weight, immersed in an ice−water bath. The vapor pressure of HNO_3 for this solution at 273 K is 0.20 Torr.[20]

Chemical Ionization Mass Spectrometric Detection. A proton-transfer chemical ionization scheme was used for mass spectrometric detection of the products of the OH-initiated oxidation. For any proton acceptor B with a proton affinity higher than that of water (PA = 165 kcal mol^{-1}),[21] the following reaction usually occurs near the collisionally limited rate

$$H^+(H_2O)_n + B \rightarrow BH^+(H_2O)_{n-m} + mH_2O \qquad (13)$$

Water cluster ions corresponding to a value of $n = 4$ typically accounted for more than 80% of the total ion signal produced in the ionization source and small amounts of $n = 3$ and 5 were also observed. Protonated water clusters were produced in the ionization source by passing a large N_2 flow (prepurified; 8 STP L min^{-1}) through the ^{210}Po α-particle-emitting ionization source, with H_2O impurities being sufficient to provide a high ion signal. The commercial ionization source (NRD) consisted of a hollow, cylindrical (69 × 12.7 mm) aluminum body with 10 mCi (3.7 × 10^8 disintegrations s^{-1}) of ^{210}Po coated on the interior walls.

Species Identification. Mass spectra of the OH-initiated oxidation of 2-butyne, propyne, and acetylene were obtained. The alkyne to be studied was added to the flow reactor as a dilute mixture, simultaneously with oxygen, through a sidearm. Due to differing OH reactivities, 2-butyne (99%) and propyne (98%) were added as 5% and 7% mixtures in N_2, respectively, and acetylene (98.5+%) was added as a 50% mixture in N_2. Mass scanning occurred between 30 and 210 *m*/*z*. Peak assignments were evaluated and tested by ensuring that the peak behavior under different conditions (e.g., turning the OH radical, alkyne, or oxygen source on and off) showed the correct reactant dependence.

Biacetyl and Acetic Acid Calibration Mass Spectrometric Calibration. Standard samples of biacetyl (97%) for mass spectrometric calibration were commercially obtained and prepared by drawing appropriate amounts of biacetyl vapor from the liquid sample and mixing them with N_2 to make 0.5% biacetyl/N_2 mixtures. Acetic acid samples were delivered using a trap method during calibrations due to the low vapor pressure of acetic acid at room temperature and due to the difficulty involved in preparing accurate gas mixtures below concentrations of 0.5%. Thus, samples were delivered into the mass spectrometer by flowing metered N_2 through a trap containing glacial acetic acid (99.8%).

Product-Forming Kinetics for the 2-Butyne System. 2-Butyne was added into the main flow tube as a 5% 2-C_4H_6/N_2 upstream of the OH source, as is shown in Figure 1. Known amounts of O_2 were added through the movable injector by flow metered delivery of a 20% O_2 (99.98%)/N_2 mixture. The product-forming kinetics of the 2-butyne-OH + O_2 reaction was measured by directly observing the production of biacetyl and acetic acid, the two major stable products of the reaction. Biacetyl and acetic acid production were monitored over a reaction time of ∼30 ms, which was calculated from the flow velocity and the distance between the injector and the mass spectrometer sampling aperture.

Computational Methods

Modified G2MS Method. Geometries and relative energies of relevant reactants, intermediates, products, and chemical ionization products in each reaction system were calculated using a modified version of the G2MS compound method (MG2MS),[22] a variation on G2 theory, using Gaussian 98 software.[23] Each stationary point was confirmed as a potential energy minimum by inspection of the calculated frequencies.

The overall energy expression for the MG2MS scheme is defined in eq 14

$$E_{\mathrm{G2MS}} = E_{\mathrm{CCSD(T)/6-31G(d)}} + E_{\mathrm{MP2/6-311+G(2df,2p)}} - E_{\mathrm{MP2/6-31G(d)}} + \mathrm{HLC} \quad (14)$$

where HLC is an empirically defined correction term with HLC $= An_\alpha + Bn_\beta$ where n_α and n_β are the number of α and β electrons, respectively, and the constants A and B are 6.06 and 0.19 mH, respectively. Our previous MG2MS results for atmospherically relevant systems (including radicals and ions) indicate that the MG2MS calculated thermodynamic properties (enthalpies of reaction) are typically accurate to within 2.5 kcal mol^{-1} for systems similar to those under study here.[24]

Transition State Energy Calculations. Transition state structures of molecules of interest were located using B3LYP/6-31G(d,p) optimizations and confirmed as first-order saddle points by inspection of the number of calculated imaginary frequencies. Intrinsic reaction coordinate (IRC) calculations were used to verify that each structure was a transition state for the proposed reaction. Energies of the transition states were also calculated using the MG2MS method.

Results and Discussion

Chemical Ionization Schemes. In order for the proton-transfer chemical ionization method to detect the species of interest, the proton affinity of each species must be higher than the proton affinity of H_2O (PA = 165 kcal mol^{-1}). However, with the exception of formic (PA = 177 kcal mol^{-1}) and acetic (PA = 187 kcal mol^{-1}) acid,[21] the experimental proton affinities of the other species of interest have not been measured. Standard enthalpies of reaction for the relevant proton transfer reactions (for all species previously observed or expected as reaction intermediates in the oxidation of acetylene) were therefore computed using the G2MS method and the results are shown in Table 1. Since all of the computed enthalpies of reaction are more negative than the proton affinity of H_2O (although for glyoxal, it is within the estimated error of the calculations), it is expected that all species should be detected by proton-transfer chemical ionization mass spectrometry methods. Our past experience with similar closed shell oxygenated hydrocarbons and hydroxy and peroxy radicals[14,25−28] indicate that such species can be detected at about the 100 ppt level (or 3×10^9 molecule cm^{-3} at 100 Torr) with the TF−CIMS technique. Since the approximate initial OH concentrations in these experiments were determined to be $\sim 1 \times 10^{11}$ molecule cm^{-3}, signal-to-noise ratios for the species of interest are expected to be on the order of 30:1. Therefore, the proton transfer technique is expected to be capable of uniquely and sensitively detecting all important intermediate and final oxidation products for acetylene. Similar calculations were carried out for species related to the 2-butyne oxidation, and in every case, the proton-transfer reactions are predicted to be even more exothermic than for the acetylene oxidation system.

Species Identification Experiments. To ensure optimum conditions for the species identification experiments, gas concentrations and flow rates were adjusted to optimize the detection of intermediates and final products at the mass spectrometer. Radical-forming reactions in the sidearm were allowed to reach completion before entering the main flow tube in order to minimize unwanted secondary chemistry. Because the OH reaction rate constant increases dramatically as the alkyne chain lengthens (from 8.8×10^{-13} cm^3 $molecule^{-1}$ s^{-1} for acetylene to 3.0×10^{-11} cm^3 $molecule^{-1}$ s^{-1} for 2-butyne),[17] much lower 2-butyne concentrations could be used in the experiments as compared to acetylene. Consequently, the 2-butyne system was the least susceptible to secondary chemistry interferences and was thus the subject of the most extensive experimental investigation.

TABLE 1: MG2MS Standard Enthalpies of Reaction (in kcal mol^{-1}) for Proton Transfer Processes of Species Related to the Oxidation of Acetylene

	$\Delta_r H$
(1) HC−C(OH)H + H^+ → $C_2H_2^+$ + H_2O	−172
(2) H_2C−C(=O)H + H^+ → H_2C−C(=OH^+)H	−183
(3) HC(OO)-C(OH)H + H^+ → HC(OOH^+)-C(OH)H	−201
(4) HC(OOH)-C(O)H + H^+ → HC(OOH^+)-C(OH)H	−194
(5) HC(=O)-C(=O)H + H^+ → HC(=OH^+)-C(=O)H	−167

Species Identification Results for 2-Butyne System. Because the proton-transfer reaction for the alkyne-OH adduct is expected to produce an alkyne cation and H_2O (see Reaction 1 in Table 1), attempts were made to detect $C_4H_6^+$ and its hydrates for experiments conducted with 2-butyne in the absence of oxygen. However, a high background signal was observed at these *m*/*z* ratios. This was probably due to the relatively high concentrations of 2-butyne in the flow reactor, which itself may be partially ionized by other ion-forming processes (such as 2-C_4H_6 + O_2^+ → 2-$C_4H_6^+$ + O_2). Therefore, the definitive detection of the 2-C_4H_6−OH adduct by proton-transfer CIMS methods was inconclusive. However, despite the favorable proton transfer thermodynamics and expected signal-to-noise ratios of 30:1 (as discussed above), neither the 2-butyne-derived vinoxy radical (a proposed isomerization product of the 2-butyne-OH adduct)[16] nor the 2-butyne-derived hydroxy peroxy radical were observed in experiments performed in the presence of O_2. Instead, the OH-initiated oxidation of 2-butyne yielded only biacetyl and acetic acid as identifiable oxidation products, in agreement with the results of Hatakeyama et al.[17] Biacetyl was observed principally at 141 *m*/*z* ($H^+C_4H_6O_2 \cdot 3H_2O$), though it was also observed at 123 *m*/*z* ($H^+C_4H_6O_2 \cdot 2H_2O$). Acetic acid was observed principally at 97 *m*/*z* ($H^+CH_3COOH \cdot 2H_2O$), and it was also observed at 115 *m*/*z* ($H^+CH_3COOH \cdot 3H_2O$).

Species Identification Results for Propyne System. Similar to findings for the 2-butyne system, the CIMS data were inconclusive with respect to the presence of C_3H_6−OH adduct in the absence of oxygen. The vinoxy isomerization product and the propyne-derived hydroxy peroxy radical again were not detected with the proton-transfer CIMS method. In agreement with Hatakeyama et al., methylglyoxal and acetic acid were observed as major products.[17] Methylglyoxal was observed primarily at 127 *m*/*z* ($H^+C_3H_4O_2 \cdot 2H_2O$), and acetic acid, as in the 2-butyne case, was observed principally at 97 *m*/*z* ($H^+CH_3COOH \cdot 2H_2O$) and also at 115 *m*/*z* ($H^+CH_3COOH \cdot 3H_2O$). Evidence for the production of formic acid was observed in the form of formic acid dimer at 111 *m*/*z* ($H^+(HCOOH)_2 \cdot H_2O$) and 129 *m*/*z* ($H^+(HCOOH)_2 \cdot 2H_2O$), contrary to the results of Hatakeyama et al. in the oxidation of propyne, in which no formic acid was observed.

Species Identification Results for Acetylene System. The acetylene experiments were the most difficult to interpret, because of the high acetylene concentrations required to drive the OH + acetylene reaction to completion. Under these high acetylene concentrations, several peaks at large *m*/*z* ratios were observed, which suggests that chain polymerization may have been occurring, which has been observed for the Cl-initiated oxidation of acetylene.[29] Again, the high acetylene concentrations made the attempt to identify the C_2H_2−OH adduct via CIMS methods inconclusive. As for the 2-butyne and propyne

TABLE 2: MG2MS Relative Energies (in kcal mol^{-1}) of Reactants, Intermediates, and Products of OH-Initiated Alkyne Oxidation[a]

	C_2H_2	C_3H_4	2-C_4H_6	C_2H_4
free C_xH_y + OH + O_2	0	0, 0	0	0
C_xH_y-OH adduct	−26	−28, −29	−29	−24
four-membered ring	−57	−59, −59	−62	
three-membered ring	−59	−70, −68	−70	
hydroxy peroxy radical	−74	−76, −76		−57
oxy peroxide radical	−81	−83, −83	−84	−36
α-dicarbonyl + OH	−104	−107, −107	−112	
carboxylic acid + carbonyl radical	−136	−143, −138	−145	

[a] The paired values for C_3H_4 indicate energies for the terminal (left) and central (right) addition of OH.

systems, the vinoxy isomerization species and the acetylene-derived hydroxy peroxy radical were not observed. Instead, the OH-initiated oxidation of acetylene yielded glyoxal as the major product, again in agreement with previous studies. Glyoxal was observed primarily at 95 *m*/*z* ($H^+C_2H_2O_2 \cdot 2H_2O$) and formic acid (in the form of formic acid dimer) was observed at 129 *m*/*z* ($H^+(HCOOH)_2 \cdot 2H_2O$).

In summary, in no case was the vinoxy isomerization species (proposed by Schmidt et al. to form from the alkyne-OH adduct[16]) observed, and in no case was the hydroxy peroxy radical observed over the 30 ms time scale of the experiment, despite the expectation that the proton-transfer CIMS methods should be quite sensitive and selective for these species. Instead, a mechanism that forms an α-dicarbonyl compound (biacetyl, methylglyoxal, and glyoxal) and a carboxylic acid (acetic acid and formic acid) seems to dominate. These species identification results are in good agreement with product studies of Hatakeyama et al.,[17] but it is important to note that our experiments set a much lower limit on the time scale of these product forming processes and provide constraints on the identities and/or lifetimes of the proposed intermediates. A quantitative determination of the final product-forming time scales for the 2-butyne system is described in a subsequent section.

Computational Results. Calculated energies of reactants and potential oxidation intermediates and products for the series of alkynes studied (for sequential reaction with OH and O_2, respectively) are presented in Table 2. The results have been placed on a relative energy scale, with the sum of the energies of the free reactants as the reference. Vinoxy isomerization species were not included in the results because none were experimentally observed in any of the reaction systems, and it is much more likely that the alkyne-OH adduct is the actual intermediate species for OH addition to the alkyne. It is notable that the energetics of the various stages of oxidation depend very little on the identity of the parent alkyne. The generalized diagram in Figure 2 shows the relative energies schematically. Not surprisingly, Figure 2 reveals that the experimentally observed α-dicarbonyl and carboxylic acid product-forming channels are strongly thermodynamically favored and that they differ mechanistically due to the O_2 reaction step (e.g., both product channels derive from the alkyne-OH adduct). However, the calculations do suggest that the formation of unusual

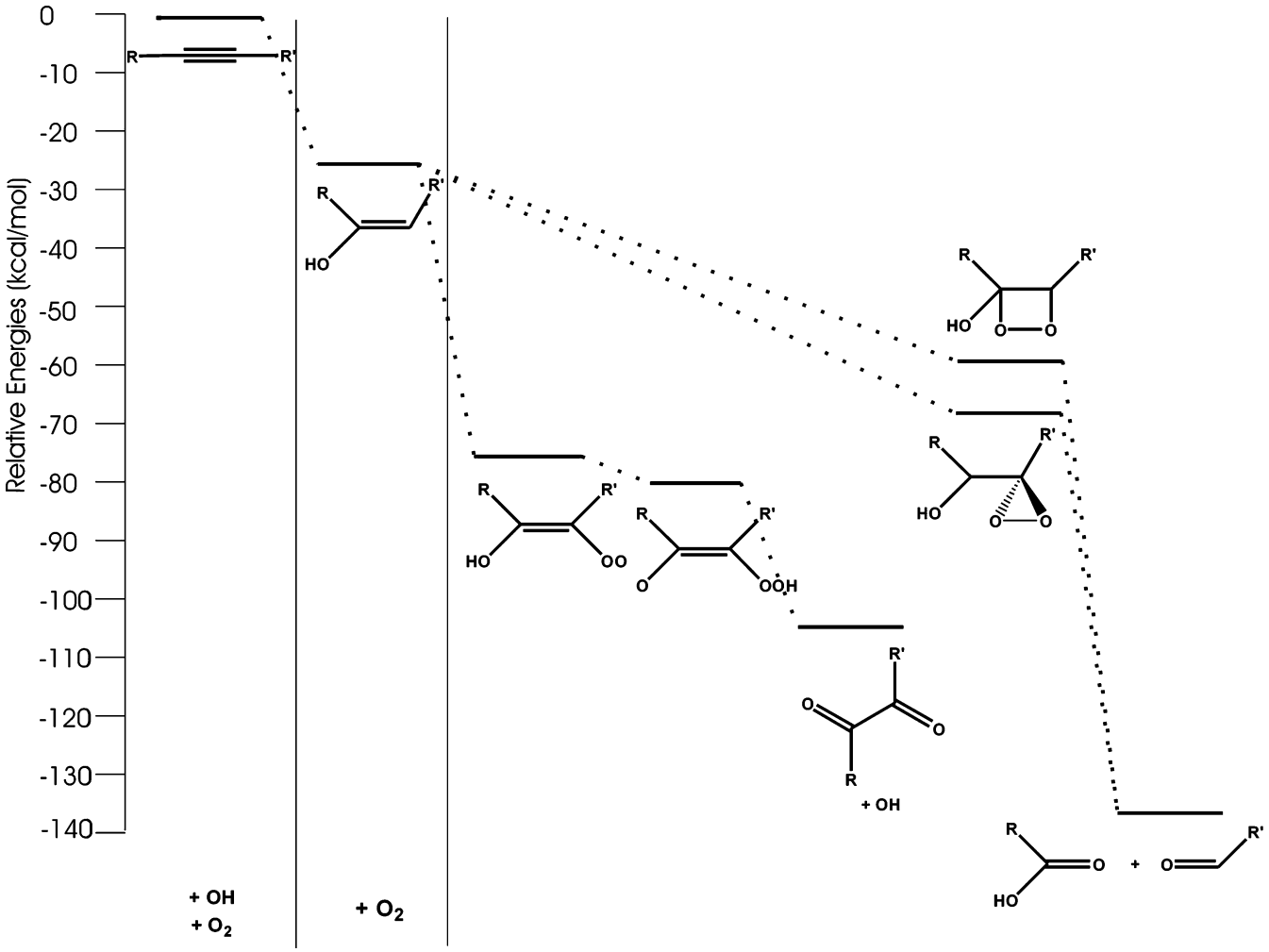

Figure 2. Diagram of the relative energies of alkyne oxidation reactants, intermediates, and products.

intermediate species is the likely explanation for the identities of the observed products.

The most favorable thermodynamic pathway is the formation of a carboxyl acid and a radical carbonyl compound. Figure 2 shows two possible intermediate species that could potentially lead to these products: a four-membered cyclic intermediate originally proposed by Hatakeyama et. al.[17] and three-membered cyclic intermediate. Carpenter proposed a similar three-membered cyclic intermediate in the reaction of vinyl radical with O_2 in an attempt to rationalize the experimentally observed products.[30] Carpenter pointed out that the four-membered cyclic intermediate must rotate 90° about the C−C bond to achieve ring closure. Since the C−C bond retains π-bonding character, this rotation would be expected to drive up the energy of the four-membered ring species. Carpenter showed that this energy cost for the four-membered ring closure is greater than the energy cost of the three-membered ring closure (which, although there is undoubtedly more steric ring strain, does not require any torsional motion), and thus, the three-membered ring is energetically favored for the vinyl-O_2 species. Of course, transition state theory calculations would be required to prove that the three-membered ring intermediate is the more kinetically accessible pathway. In any case, our G2MS calculations also show that the three-membered ring intermediate is energetically favored over the four-membered ring species for alkyne-OH−O_2 species (although the energy difference is within the error of the calculations for the acetylene-derived species).

It is clear from our computational thermodynamic and experimental results (as well as those obtained by Hatakeyama et al.[17]) that the α-dicarbonyl product-forming pathway must be more kinetically facile than the acid-forming pathway, since it is not the thermodynamically favored pathway. Despite previous observations of the α-dicarbonyl products (and the accompanying OH regeneration), none of the previous works outlined a potential mechanism that could explain these products. Our initial calculations were aimed at characterizing the most obvious intermediate: the hydroxy peroxy radical expected to form from the addition of O_2 to the alkyne-OH adduct. Although stationary states were located for hydroxy peroxy radicals derived from acetylene and propyne, geometry optimization of the similar species for 2-butyne lead instead to an oxy peroxide radical species. Presumably, this species could form from an intramolecular H-atom transfer from the hydroxy group to the peroxy group. A previous computational study showed that hydroxy peroxy radicals derived from ethene prefer an intramolecular six-membered ring confirmation that allows hydrogen bonding between the H-atom on the hydroxy group and the terminal O-atom on the peroxy group.[31] This structure was found to be about 2 kcal mol^{-1} more favorable than one in which no intramolecular bonding occurs. We carried out a similar calculation for the hydroxy peroxy radical derived from acetylene and found that a similar intramolecular bonding situation leads to a 6 kcal mol^{-1} stabilization over one in which no intramolecular bonding occurs. Therefore, it is very likely that the alkyne-OH−O_2 species adopt confirmations which could facilitate H-atom transfer. Indeed, for all three alkynes studied, the oxy peroxide isomer was found to be more stable than the hydroxy peroxy isomer. For comparison with the alkene oxidation mechanism, similar calculations were carried out for the ethene-derived hydroxy peroxy and oxy peroxide species, and it was found that the hydroxy peroxy species was more stable by more than 20 kcal mol^{-1} (see Table 2), thus explaining the stability of hydroxy peroxy radicals formed in the oxidation of alkenes. The CCSD(T)/6-31G(d) spin densities indicate that delocalization is the likely cause of the unusual stability of the alkyne-derived oxy peroxide species. For the alkyne-derived hydroxy peroxy species, the unpaired electron is almost totally localized on the terminal peroxy oxygen atom (as is the norm for peroxy radicals), whereas for the alkyne-derived oxy peroxide species, the unpaired electron is delocalized over the oxygen atom and the two carbon atoms.

The structure of the oxy peroxide intermediate species immediately suggests an explanation for the experimental product observations: dissociation of the weak O−O bond in the peroxide group to produce OH and the α-dicarbonyl product. Indeed, the highest occupied molecular orbital for the oxy peroxide species was found to possess significant π-antibonding O−O character. As described above, the computational results suggest that there is no barrier between the hydroxy peroxy and oxy peroxide species for the 2-butyne case. A transition state for the similar isomerization process for the acetylene system was located and possessed an energy only 0.6 kcal mol^{-1} above that for the hydroxy peroxy species. Therefore, it seems likely, given the experimental and computational results, that the hydroxy peroxy species is very short-lived and that it is the oxy peroxide species that leads directly to the observed α-dicarbonyl products and OH regeneration. The proton transfer chemical ionization method should also be able to detect the oxy peroxide species (see reaction 4 in Table 1) at the same *m*/*z* ratios expected for the hydroxy peroxy species. Since this potential observation was reported earlier as a negative result on the 30 ms experimental time scale, it is apparent that both the hydroxy peroxy and oxy peroxide species must be relatively short-lived.

Proposed Alkyne Oxidation Mechanism. Based on the mass spectrometric product analyses and the computational results on the relevant reactants, intermediates, transition states, and products, a general mechanism is proposed for the OH-initiated atmospheric oxidation of alkynes. Reaction 15 depicts the first step in the oxidation process, an addition of OH to one side of the triple bond.

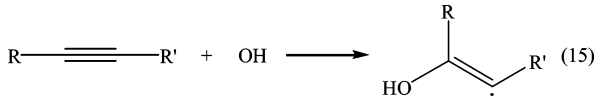

Experimental results from this study seem to rule out the isomerization of this adduct to the alkyne-derived vinoxy species, as proposed by Schmidt et al.[16] The subsequent reaction with oxygen occurs via two channels, the first of which produces a carboxylic acid and a carbonyl radical. Cyclic addition of O_2 to the π-bonding system of the alkyne likely leads to a three-membered ring intermediate in reaction 16a, which decomposes to a carboxylic acid and a carbonyl radical.

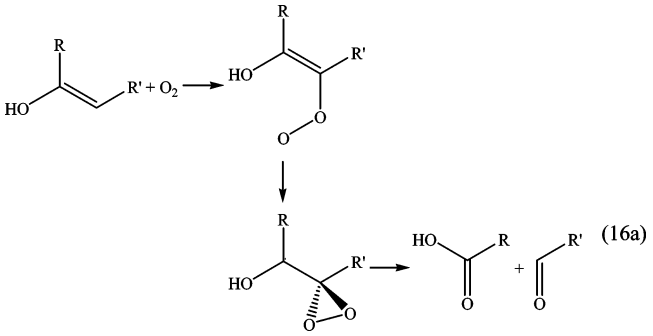

This step is different from the mechanism proposed by Hatakeyama and co-workers,[17] as the present thermodynamics

calculations indicate a three-membered ring intermediate species is more energetically feasible. The second possible addition mechanism for O_2, in reaction 16b, leads to the production of a stable α-dicarbonyl compound.

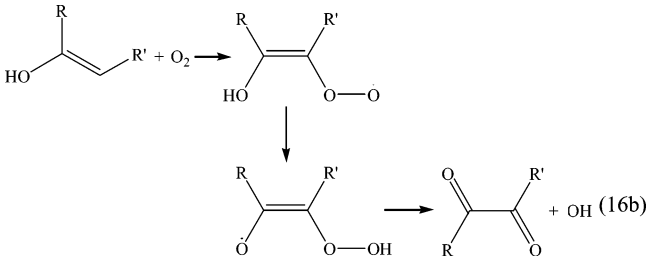

(16b)

In this mechanism, oxygen adds to the other side of the C−C bond across from the site of OH reaction, forming a hydroxy peroxy radical that rapidly isomerizes to an oxy peroxide radical through an intramolecular H-atom transfer. The resulting oxy peroxide radical then rapidly decomposes to a stable α-bicarbonyl compound and an OH radical. This hydroxy peroxy to oxy peroxide isomerization is apparently the first proposed mechanism that is able to explain the production of stable α-dicarbonyl compounds and OH regeneration resulting from the oxidation of alkynes. The experimental result that neither the hydroxy peroxy nor the oxy peroxide species were detected by CIMS methods on the time scale of the experiments (30 ms) and the computational result that the product forming pathways are likely to have relatively low barriers between intermediate species are both in strong support of a proposed mechanism in which these intermediates have very short lifetimes. To assess the atmospheric significance of the proposed alkyne oxidation mechanism with respect to tropospheric ozone production, it is important to quantitatively determine the overall rate of product formation and to confirm the branching into the two possible product channels. Therefore, the measurements of the product branching ratio and the overall product-forming rate constants for the 2-butyne system are described below.

2-Butyne-OH + O_2 Kinetics. To perform the kinetics experiments accurately, care was taken to ensure that the 2-butyne-OH adduct was formed completely before the radical synthesis components reached the O_2 injector. Kinetic traces were obtained for both biacetyl and acetic acid for O_2 concentrations ranging between 2×10^{13} and 2×10^{14} molecule cm^{-3}. Blank injector runs (in the absence of O_2) were typically taken and subtracted from product rise experiments to correct for background signal and minor reactant loss on the exposed surfaces of the injector. These data was used to determine the overall product-forming rate constants, which are discussed in more detail below. For the branching ratio determination, calibration curves were obtained for both biacetyl and acetic acid after each set of kinetics experiments were conducted in order to convert the mass spectrometer signal into absolute concentration. The biacetyl-forming branching ratio was calculated simply by calculating the ratio of biacetyl formed over a particular period of time divided by the sum of biacetyl and acetic acid formed over the same period of time. Since the greatest source of uncertainty in the measurement arises from the calibration step (as determined from the statistical uncertainty in the calibration slope), the uncertainty in the branching ratio was calculated by propagating the uncertainty of the absolute concentration obtained from the calibration curve. Our biacetyl-forming branching ratio value (0.86 ± 0.11 (2σ)) is in excellent agreement with the value of Hatakeyama (0.87 ± 0.07).[17]

To analyze the overall product-forming rate constants, it is necessary to consider the operative reaction system for 2-butyne oxidation:

$$2\text{-}C_4H_6 + OH \rightarrow C_4H_6OH \quad (17)$$

$$C_4H_6OH + O_2 \rightarrow C_4H_6O_2 + OH \quad (18a)$$

$$\rightarrow CH_3COOH + C_2H_3O \quad (18b)$$

As discussed above, the initial concentration of OH was about 1×10^{11} molecule cm^{-3}, and the initial concentration of 2-butyne was 3×10^{12} molecule cm^{-3} for each experiment. Besides 2-butyne, biacetyl is the only reactive species expected to be present at concentrations above 5×10^{10} molecule cm^{-3}. Since the OH + 2-butyne rate constant is large (3×10^{-11} cm^3 $molecule^{-1}$ s^{-1})[17] relative to the OH + biacetyl rate constant (2.5×10^{-13} cm^3 $molecule^{-1}$ s^{-1})[32] and the other reactive species are present at concentrations nearly 2 orders of magnitude less than 2-butyne, there are no significant OH reactions other than reactions 17 and 18 expected to occur under these conditions. Previous measurements have shown that OH wall loss is significantly less than the pseudo first-order loss of OH due to reaction with 2-butyne (90 s^{-1}) under the turbulent flow conditions used in this work.[33] Therefore, it is expected that reactions 17 and 18 are the predominant processes controlling the concentration of OH, and thus the observed product kinetics.

In reaction 18a, OH is regenerated, which can react with excess 2-butyne through reaction 17. Depending on the amount of excess 2-butyne in the system, multiple reaction cycles can occur over the experimental time scale. Regardless of the number of reaction cycles, the product rate laws in eqs 18a and 18b for biacetyl and acetic acid, respectively, are similar, since the rate of their production depends on the same set of reactants.

$$\frac{d[C_4H_6O_2]}{dt} = k_{18a}[C_4H_6OH]_t[O_2] \quad (19)$$

$$\frac{d[CH_3COOH]}{dt} = k_{18b}[C_4H_6OH]_t[O_2] \quad (20)$$

Because the rate laws are identical (except for the bimolecular rate constants k_{18a} and k_{18b}), the following discussion of the kinetics modeling will be developed for the biacetyl case, with the understanding that the same analysis can be applied to acetic acid.

If reaction 18b is neglected, it is apparent that a rigorous steady-state situation for OH and the 2-butyne-OH adduct arises from the OH regeneration due to reaction 18a. In reality, the 2-butyne-OH + O_2 reaction follows the reaction 18b pathway 14% of the time. Because the reaction 18b product channel is chain terminating for OH, the steady state condition for OH does not rigorously apply. Nonetheless, if reaction 18b is neglected for the moment, and 2-C_4H_6 is assumed to be in excess, a rate law can be derived beginning with a steady-state approximation for OH

$$\frac{d[OH]}{dt} = -k_{17}[2\text{-}C_4H_6]_0[OH]_t + k_{18a}[C_4H_6OH]_t[O_2] \approx 0 \quad (21)$$

Solving for $[C_4H_6OH]_t$

$$[C_4H_6OH]_t = \frac{k_{17}[2\text{-}C_4H_6]_0[OH]_t}{k_{18a}[O_2]} \quad (22)$$

Because of the approximate steady-state condition, a mass

balance between OH and the 2-butyne-OH adduct can also be inferred, which yields eqs 23 and 24

$$[OH]_t + [C_4H_6OH]_t \approx [OH]_0 \quad (23)$$

$$[OH]_t \approx [OH]_0 - [C_4H_6OH]_t \quad (24)$$

Substituting eq 24 into eq 22 and solving for $[C_4H_6OH]_t$

$$[C_4H_6OH]_t = \frac{k_{17}[2\text{-}C_4H_6]_0[OH]_0}{k_{17}[2\text{-}C_4H_6]_0 + k_{18a}[O_2]} \quad (25)$$

By substituting the result from eq 25 back into the rate law (eq 19), an equation describing the dependence of the biacetyl production rate on oxygen is obtained

$$\frac{d[C_4H_6O_2]}{dt} = \frac{k_{18a}[O_2]\, k_{17}[2\text{-}C_4H_6]_0[OH]_0}{k_{17}[2\text{-}C_4H_6]_0 + k_{18a}[O_2]} \quad (26)$$

or, grouping the constant terms

$$\frac{d[C_4H_6O_2]}{dt} = \frac{A[O_2]}{B + C[O_2]} \quad (27)$$

At low $[O_2]$, the $C[O_2]$ term is small compared to the B term, and the rate of production of biacetyl will have a linear dependence on O_2. As $[O_2]$ increases, the $C[O_2]$ becomes large compared to B and the rate of production of biacetyl will eventually reach a constant value. Since for any given experiment, $[O_2]$ is a constant, the integrated form of eq 27 is trivial

$$[C_4H_6O_2]_t = Dt \quad (28)$$

where D is a constant.

However, if $[O_2]$ is large enough, the product curves will deviate from this linear, steady-state behavior due to the increasing effect of the acetic acid channel (reaction 18b), which can be exacerbated by the concurrently increasing degree of OH regeneration. Each OH regeneration cycle compounds the deviation from linearity because the approximations in eqs 21 and 23 become increasingly inaccurate. Therefore, the O_2 concentrations were chosen such that eq 28 remained approximately valid, as indicated by full kinetic modeling of the reaction system (e.g., no steady-state assumption used).

Figure 3 shows the experimentally determined time dependences of biacetyl production for a range of oxygen concentrations fit to the linear model derived from the steady-state model (eq 28). Figure 4 presents the expected biacetyl production kinetics traces under the same conditions using the full kinetics model with no steady-state assumptions. It is clear from the similarity of Figures 3 and 4 that eq 28 approximates the observed kinetics quite closely.

To reduce the number of fitting parameters, eq 27 was approximated by the following exponential function (which has the same limiting behavior as eq 27):

$$\frac{d[C_4H_6O_2]}{dt} = (1 - e^{-k_{eff}[O_2]}) \quad (29)$$

In this model, there is only one variable parameter, k_{eff}, and absolute concentration data for biacetyl and acetic acid are not required to analyze the data, obviating the need for difficult calibration experiments. The biacetyl product formation rates (the slopes of the lines from Figure 3) were scaled so that the maximum value was set to unity and were then plotted vs $[O_2]$

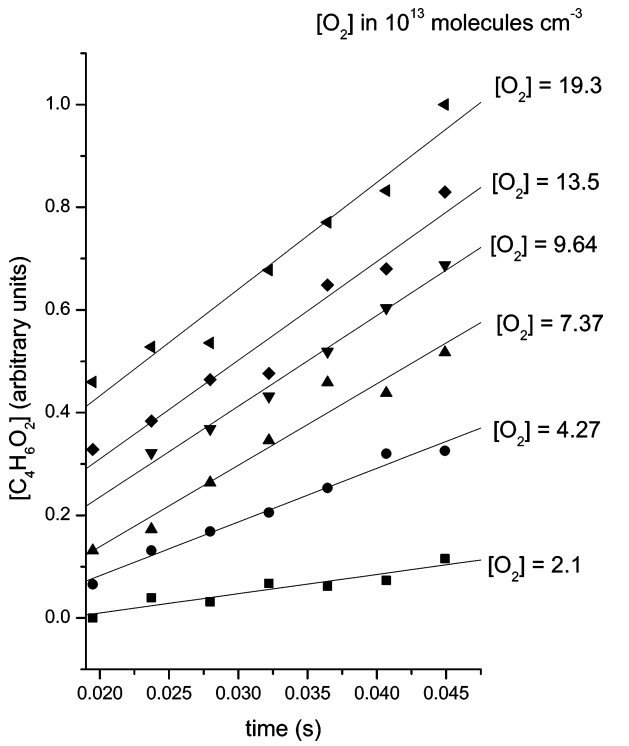

Figure 3. Biacetyl production data for the 2-butyne-OH + O_2 reaction at 100 Torr, 298 K, 1180 cm s^{-1} flow velocity, and 2240 *Re* fit with approximate steady-state linear production model.

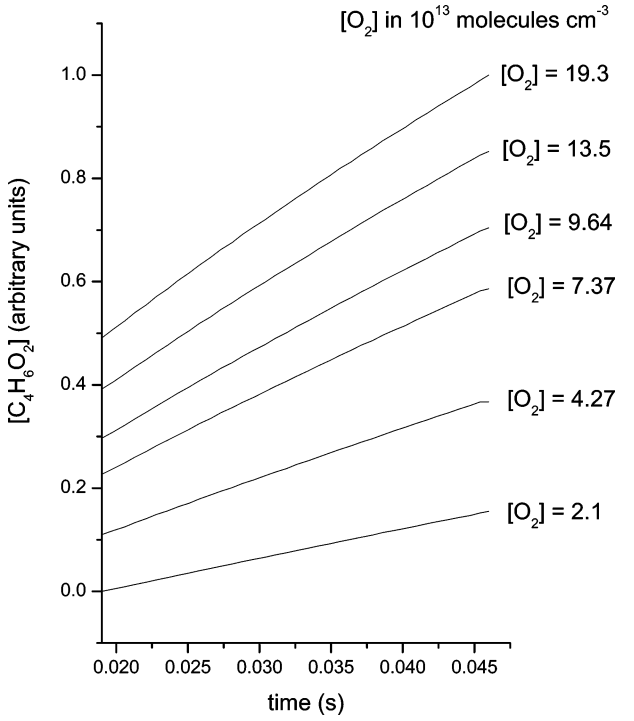

Figure 4. Modeled biacetyl production for conditions in Figure 3 with rigorous kinetic treatment (no steady-state assumption).

as shown in Figure 5. The steady-state model result for the oxygen dependence of the production rates (eq 29) was used to fit the data (shown in Figure 5 as a solid line). The full kinetics model was also used to predict the oxygen dependence of the biacetyl production (presented in Figure 5 as a dashed line), and it is apparent that the steady-state model provides a good description of these data as well. The data collected for the acetic acid production experiments were analyzed according to eq 28

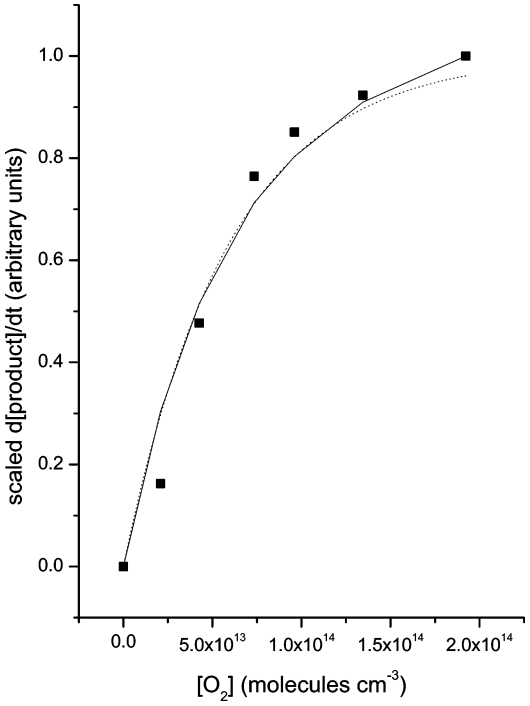

Figure 5. Biacetyl production rate as a function of oxygen concentration (from data in Figure 3) fitted with approximate steady-state model (solid line) and modeled results from rigorous kinetic treatment (dashed line).

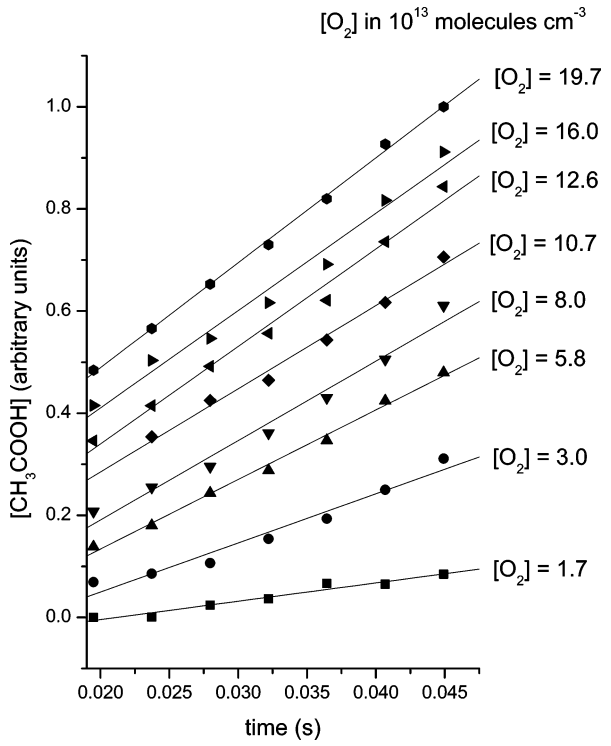

Figure 6. Acetic acid production data for the 2-butyne-OH + O_2 reaction at the same conditions as Figure 3 with approximate steady-state linear production model.

and are presented in Figure 6. As expected from the full kinetics model, the product formation rates as a function of $[O_2]$ were found to be identical for both biacetyl and acetic acid, as shown in Figure 7, and were simultaneously fit to eq 29 to determine a single k_{eff} value.

Next, full kinetics modeling was carried out with assumed values for the individual rate constants (k_{17}, k_{18a}, and k_{18b}). The

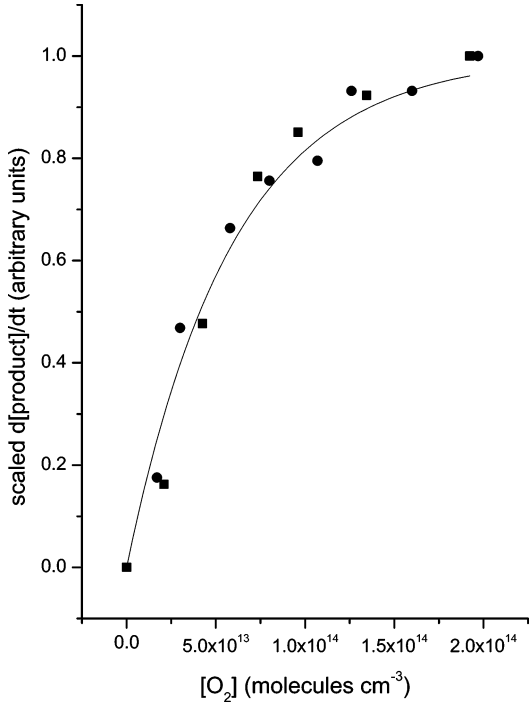

Figure 7. Biacetyl (squares) and acetic acid (circles) production data as a function of oxygen concentration (from data in Figures 3 and 6) fitted with approximate steady-state model.

k_{17} rate constant was fixed to the value (3×10^{-11} cm^3 molecule^{-1} s^{-1}) determined by Hatakeyama et al.[17] The modeled results (d[$C_4H_6O_2$]/dt vs $[O_2]$) were then fitted with eq 29 to determine a model k_{eff} value. The process was then iterated by varying k_{18a} and k_{18b} (but holding their relative values constant according to our branching ratio measurement) until the modeled k_{eff} was equal to the k_{eff} determined experimentally. An overall rate product formation rate constant, k_{18}, was determined to be 7.04 ± 0.60 (2σ) x 10^{-13} cm^3 molecule^{-1} s^{-1}. The statistical uncertainties were propagated from the uncertainties in the fitting process described above. The turbulent flow method assumes that deviations from the plug flow approximation (molecular velocities are equal to the bulk flow velocity) are negligible. Under the conditions present in the turbulent flow tube ($Re >$ 2000), Seeley and co-workers estimated that these deviations result in apparent rate constants which are at most 8% below the actual values.[33] The other likely systematic errors in the determination of rate constants are likely to occur in the measurements of gas flows, temperature, detector signal, and pressure. Considering these errors and the errors involved in the branching ratio measurements, k_{18} is estimated to be accurate to within $\pm$30% (2σ).

To the best of our knowledge, no data exists in the literature for the direct measurement of the rate of reaction 18. Seise and Zetzsch, however, used OH cycling methods to determine the glyoxal + OH forming rate constant for the acetylene-OH + O_2 reaction.[18] The value reported in that work was $4.2 \pm 0.5 \times 10^{-12}$ cm^3 molecule^{-1} s^{-1}. This value is substantially higher than the overall product-forming rate constant determined for the 2-butyne-OH + O_2 reaction in this work.

Atmospheric Implications. The overall rate constant for the reaction of the 2-butyne-OH adduct with O_2 and the concentration of oxygen at atmospheric pressure ($[O_2] = 4.9 \times 10^{18}$ molecule cm^{-3}) can be used to determine the atmospheric lifetime of the 2-butyne-OH adduct. Based on these values, the atmospheric lifetime of the 2-butyne-OH adduct is a mere 0.29 μs. Using the 2-butyne + OH rate constant determined by

Hatakeyama et al. (3.0×10^{-11} cm^3 molecule^{-1} s^{-1})[17] and a diurnally averaged OH concentration of 5×10^5 molecule cm^{-3}, the atmospheric lifetime of 2-butyne with respect to reaction with OH is about 18 h. Therefore, the initial oxidation step (alkyne + OH) completely controls the rate of alkyne oxidation in the atmosphere. Although it is possible that the time scale of the present experimental method was too long to observe any hydroxy peroxy radical intermediates formed in the oxidation of alkynes, it is of interest to consider whether such short-lived hydroxy peroxy radicals might react with NO and produce NO_2 under certain atmospheric conditions, and thus contribute directly to tropospheric ozone production. Assuming highly polluted tropospheric NO levels of 100 ppb (1.6×10^{12} molecule cm^{-3}) and a rate constant of 9×10^{-12} cm^3 molecule^{-1} s^{-1} (similar to the values determined for the reaction of NO with a series of alkane- and alkene-derived hydroxy peroxy radicals),[13,14] the lifetime of a hypothetical 2-butyne-derived hydroxy peroxy radical with respect to NO reaction is predicted to be about 70 ms, more than 5 orders of magnitude slower than the rate at which a 2-butyne-OH radical is converted into stable oxidation products by reaction with O_2. The experimental and computational results strongly suggest that oxidations of propyne and acetylene are likely to be similar to that of 2-butyne (differing significantly only in the rate of the initial OH reaction). Consequently, since any alkyne-derived hydroxy peroxy radicals are probably not long-lived enough to react with NO, the primary alkyne oxidation sequence does not appear to lead to tropospheric ozone production, thus setting this chemical class apart from the vast majority of atmospherically abundant hydrocarbons.

Although the hydroxy peroxy + NO reaction may not be operative in the primary atmospheric oxidation sequence of alkynes, secondary oxidation of the primary oxidation products may contribute significantly to tropospheric ozone production. For example, in the acetic acid forming channel for the 2-butyne oxidation, an acetyl radical is also formed. In the presence of oxygen, this species will form an acetyl peroxy radical, which is known to be highly reactive with NO.[13] The secondary peroxy radicals formed from this process can be directly predicted from the acid-forming branching ratios determined by Hatakeyama: 40%, 12%, and 14% for acetylene, propyne, and 2-butyne oxidation,[17] respectively. Therefore, it seems that alkyne oxidation can contribute to tropospheric ozone production in a secondary fashion through the minor, acid-forming channel.

The atmospheric fates of α-dicarbonyls related to alkyne oxidation were investigated by Plum et al.[34] Using measurements of the OH rate constant and photolysis rates, Plum et al. concluded that the α-dicarbonyl lifetimes against OH ranged from 24 h for glyoxal to more than 900 h for biacetyl, whereas the lifetimes against photolysis ranged from 5 h for glyoxal to 1 h for biacetyl. Therefore, photolysis appears to be the major atmospheric removal process for α-dicarbonyls. Plum et al. concluded that there were two major photolysis pathways

$$O{=}HC{-}CH{=}O + h\nu \rightarrow H_2C{=}O + CO \qquad (30)$$

$$O{=}HC{-}CH{=}O + h\nu \rightarrow 2CO + H_2 \qquad (31)$$

More recent work has indicated that a third channel could be important[35]

$$O{=}HC{-}CH{=}O + h\nu \rightarrow 2HCO \qquad (32)$$

Although the products of reactions 30 and 31 are relatively long-lived in the atmosphere, the product of reaction 32 would be quickly converted in the atmosphere to HO_2, which would facilitate the NO to NO_2 conversion necessary for ozone production. Therefore, unless reaction 32 is dominant fate of glyoxal in the atmosphere, it is likely that the α-dicarbonyl-producing alkyne oxidation channel contributes only in a minor fashion to the production of tropospheric ozone.

Therefore, in contrast to the alkanes and the alkenes, atmospheric alkynes appear to play a much smaller role in tropospheric ozone production. Atmospheric alkanes and alkenes contribute to ozone formation through the formation of peroxy radicals in the primary oxidation sequence. In contrast, atmospheric alkynes do not appear to contribute to ozone formation at all in their primary oxidation sequence, due to the lack of long-lived peroxy radicals; however, some ozone formation might result from secondary oxidation reactions.

Recently, remote sensing of glyoxal has been used as a new atmospheric tracer for volatile organic compound chemistry and secondary organic aerosol formation in a Mexico City field study.[36] The primary source of glyoxal in the atmosphere has been previously identified as arising from the photooxidation of aromatic compounds,[37] and typical urban concentrations are on the order of 0.04−0.3 ppb.[38] Using the acetylene + OH rate constant (8.8×10^{-13} cm^3 molecule s^{-1}) and glyoxal branching ratio (0.70) as determined by Hatakeyama et al.,[17] an average daytime OH concentration of 0.04 ppt (1×10^6 molecule cm^{-3}), an urban acetylene concentration[12] of 17 ppb (4×10^{11} molecule cm^{-3}), and the finding in this work that the conversion of the acetylene-OH adduct to glyoxal occurs virtually instantaneously in the atmosphere, a daytime glyoxal production rate of 0.05 ppb/hr is obtained, which is on the same order as the *average* daytime glyoxal concentration. Therefore, it seems likely that the oxidation of acetylene is a significant source of glyoxal in the urban atmosphere.

Conclusions

The mechanism and kinetics of the atmospheric oxidation of alkynes have been studied at 100 Torr and 298 K, with particular attention paid to the potential for alkyne oxidation to contribute to tropospheric ozone formation. The major products of OH-initiated oxidation of 2-butyne, propyne, and acetylene were determined using CIMS methods and the observed products were in general agreement with earlier environmental chamber FTIR results.[17] Thermodynamics calculations were used to aid the development of a general mechanism for OH-initiated oxidation of alkynes. The product branching ratio of the 2-butyne-OH adduct reaction with O_2 was determined to be 86 ± 11% biacetyl and 14 ± 11% acetic acid (2σ uncertainties reported for both), which was in excellent agreement with previous studies.[17] Conversion of the 2-butyne-OH adduct to biacetyl and acetic acid through reaction with oxygen was measured to have an overall product-forming rate constant of 7.04 ± 0.60 (2σ) $\times 10^{-13}$ cm^3 molecule^{-1} s^{-1}, which sets a very low limit on the atmospheric lifetime of peroxy radicals derived from 2-butyne. In general, the significance of atmospheric alkynes to the formation of tropospheric ozone was found to be smaller than that of the alkanes and alkenes, due to the absence of the hydroxy peroxy-forming product channel in the OH-initiated atmospheric oxidation of alkynes.

Acknowledgment. This material is based upon work supported by the National Science Foundation under Grant No. 0352537 and a Henry Dreyfus Teacher-Scholar Award. M.J.E. acknowledges useful conversations with Profs. G. B. Ellison, J.-L. Jimenez, and J. F. Stanton.

References and Notes

(1) Finlayson-Pitts, B. J.; Pitts, J. N. *Chemistry of the Upper and Lower Atmosphere*; Academic Press: San Diego, CA, 2000.
(2) Greenberg, J. P.; Zimmerman, P. R.; Heidt, L.; Pollock, W. *J. Geophys. Res.* **1984**, *89*, 1350.
(3) Greenberg, J. P.; Zimmerman, P. R. *J. Geophys. Res.* **1984**, *89*, 4767.
(4) Hegg, D. A.; Radke, L. F.; Hobbs, P. V.; Rasmussen, R. A.; Riggan, P. J. *J. Geophys. Res.* **1990**, *95*, 5669.
(5) Blake, N. J.; Blake, D. R.; Sive, B. C.; Rowland, F. S.; Collins Jr., J. E.; Sachse, G. W.; Anderson, B. E. *J. Geophys. Res.* **1996**, *101*, 24151.
(6) Stephens, E. R.; Burleson, F. R. *J. Air Pollut. Control Assoc.* **1967**, *17*, 147.
(7) *Publication No. DTS-76-2*; Mayrsohn, H., Crabtree, J. H., Kuramoto, M., Sothern, R. D., Mano, S. H., Eds.; California Air Resources Board, Division of Technical Services: Sacramento, CA, 1975.
(8) *EPA Contract No. 68-02-1735 Final Report*; Trijonis, J. C., Arledge, K. W., Eds.; TRW Environmental Services: Redondo Beach, CA, 1975.
(9) Fraser, M. P.; Cass, G. R.; Simoneit, B. R. *Environ. Sci. Technol.* **1998**, *32*, 2051.
(10) Kanakidou, M.; Bonsang, B.; Le Roulley, J. C.; Lambert, G.; Martin, D.; Sennequier, G. *Nature* **1998**, *333*, 51.
(11) Rudolph, J.; Enhalt, D. H. *J. Geophys. Res.* **1981**, *86*, 11959.
(12) Calvert, J. G.; Atkinson, R.; Kerr, J. A.; Madronich, S.; Moortgat, G. K.; Wallington, T. J.; Yarwood, G. *The Mechanisms of Atmospheric Oxidation of the Alkenes*; Oxford University Press: New York, 2000.
(13) Eberhard, J.; Howard, C. J. *J. Phys. Chem.* **1997**, *101*, 3360−3366.
(14) Miller, A. M.; Yeung, L. Y.; Kiep, A. C.; Elrod, M. J. *Phys. Chem. Chem. Phys.* **2004**, *6*, 3402.
(15) Sorenson, M.; Kaiser, E. W.; Hurley, D.; Wallington, T. J.; Nielsen, O. *Int. J. Chem. Kinet.* **2003**, *35*, 191.
(16) Schmidt, V.; Zhu, G. Y.; Becker, K. H.; Fink, E. H. *Ber. Bunsen-Ges. Phys. Chem.* **1985**, *89*, 321.
(17) Hatakeyama, S.; Washida, N.; Akimoto, H. *J. Phys. Chem.* **1986**, *90*, 173.
(18) Siese, M.; Zetzsch, C. *Z. Phys. Chem.* **1995**, *188*, 75.
(19) Bohn, B.; Zetzsch, C. *J. Chem. Soc., Faraday Trans.* **1998**, *94*, 1203.
(20) Fritz, J. J.; Fuget, C. R. *Chem. Eng. Data Ser.* **1956**, *1*, 10.
(21) NIST Chemistry Webbook, http://webbook.nist.gov/chemistry/, accessed November 2004.
(22) Froese, R. D. J.; Humbel, S.; Svensson, M.; Morokuma, K. *J. Phys. Chem. A* **1997**, *101*, 227.
(23) Curtiss, L. A.; Raghavachari, K.; Redfern, P. C.; Pople, J. A. *J. Chem. Phys.* **1997**, *106*, 1063.
(24) Cappa, C. D.; Elrod, M. J. *Phys. Chem. Chem. Phys.* **2001**, *3*, 2986.
(25) Ranschaert, D. L.; Schneider, N. J.; Elrod, M. J. *J. Phys. Chem. A* **2000**, *104*, 5758.
(26) Elrod, M. J.; Ranschaert, D. L.; Schneider, N. J. *Int. J. Chem. Kinet.* **2001**, *33*, 363.
(27) Chow, J. M.; Miller, A. M.; Elrod, M. J. *J. Phys. Chem. A* **2003**, *107*, 3040.
(28) Yeung, L. Y.; Elrod, M. J. *J. Phys. Chem. A* **2003**, *107*, 4470.
(29) Wijnen, M. H. J. *J. Chem. Phys.* **1962**, *36*, 1672.
(30) Carpenter, B. K. *J. Phys. Chem.* **1995**, *99*, 9801.
(31) Vereecken, L.; Peeters, J. *J. Phys. Chem. A* **1999**, *103*, 1768.
(32) Dagaut, P.; Wallington, T. J.; Liu, R.; Kurylo, M. J. *J. Phys. Chem.* **1988**, *92*, 4375.
(33) Seeley, J. V.; Jayne, J. T.; Molina, M. J. *Int. J. Chem. Kinet.* **1993**, *25*, 571.
(34) Plum, C. N.; Sanhuesa, E.; Atkinson, R.; Carter, W. P. L.; Pitts, J. N., Jr. *Environ. Sci. Technol.* **1983**, *17*, 479.
(35) Zhu, Z.; Kellis, D.; Ding, C.-F. *Chem. Phys. Lett.* **1996**, *257*, 487.
(36) Volkamer, R. et al. American Geophysical Union National Meeting, San Francisco, CA, 2004.
(37) Tuazon, E. C.; MacLeod, H.; Atkinson, R.; Carter, W. P. L. *Environ. Sci. Technol.* **1986**, *20*, 383.
(38) Kawamura, K.; Steinberg, S.; Kaplan, I. R. *Atmos. Environ.* **2000**, *34*, 4175.